УДК 538.945

SUPERCONDUCTING DIPOLE MAGNET FOR ALICE DIMUON ARM SPECTROMETER (CONCEPTUAL DESIGN REPORT)

P.G.Akishin, E.V.Arkhipov, V.D.Bartenev, V.A.Bogdanov, V.F.Boreiko, V.I.Datskov, H.Malinowski, V.N.Pavlov, I.V.Puzynin, A.V.Shabunov, Yu.A.Shishov, G.P.Tsvineva, A.S.Vodopianov, V.Ya.Volkov, M.B.Yuldasheva, O.I.Yuldashev

The following is the conceptual design for the construction of the dimuon forward arm spectrometer magnet of the ALICE detector. The proposed solution is a superconducting dipole magnet with a central field of 0.75 T and a field integral of 2.8 T·m. The aperture of the magnet is $\theta > 9°$. A general view of the magnet is shown.

The investigation has been performed at the Laboratory of High Energies, JINR.

Сверхпроводящий дипольный магнит для димюонного плечевого спектрометра ALICE (описание концепции проекта)

П.Г.Акишин и др.

Представлен концептуальный проект магнита, входящего в передний димюонный плечевой спектрометр детектора ALICE. Предложен вариант сверхпроводящего дипольного магнита с центральным полем 0,75 Тл и интегралом поля 2,8 Тл·м. Апертура магнита по углу равна $\theta > 9°$, по диаметру — 3,8 м.

Работа выполнена в Лаборатории высоких энергий ОИЯИ.

1. Introduction

The conceptual design for the construction of the dimuon forward arm spectrometer magnet of the ALICE detector is presented [1]. The proposed solution is a superconducting dipole magnet with a central field of 0.75 T and a field integral of 2.8 T·m. The aperture of the magnet is $\theta \geq 9°$. A general view of the magnet is shown in Fig.1. The parameters of the magnet are listed in Table 1. The design is based on the ideas already presented in [2].

Table 1. Main parameters of the dipole magnet

Items	Unit	Value
Aperture diameter	m	3.85
Outer cryostat diameter	m	5.0
Total length of the cryostat	m	5.0
Winding dia. i/o	m/m	4.2/4.3
Coil length	m	4.6
Central field	T	0.75
Maximum field on conductor	T	3.0
Operating current	kA	5.0
Conductor current density	A/mm^2	58
Total Amp · turns	MA	2.7
Stored energy	MJ	27
Cold mass	t	25
Operating temperature	K	4.5
Heat loss at 4.5 K	W	50
Heat loss at 80 K	W	480
Power of the refrigerator	W	450
Yoke mass	t	650
Total magnet mass	t	700
Cooling method	indirect thermosyphon	
Features	saddle circular winding	

2. Iron Yoke

The iron yoke is assembled of long iron blocks called slabs (see Figs.1,2). The cross section of the slabs can be varied withing some limits. The dimensional variation during the production process is rather small and not critical for the arrangement. After cutting to the length during their manufacturing at the factory, the slabs still have a temperature close to 800°C. Adequate flatness of the slabs can be achieved by piling up 15 to 20 hot slabs on an even surface during the cool-down period [3].

During the assembly, the slabs are fixed by faltering welding and with the help of welded plates. If required, the welded plates can be cut by an electrical pole-axe. All of the slabs, except for the upper and lower ones, are stacked along the magnet axis close to the cryostat.

3. 3D-Field Calculations

Three-dimensional simulations of the magnetic field have been obtained using two codes. The first code is an IAMAG3D code which is based on volume integral equations [4—6]. The second code is a MSFE3D code which uses the partial differential equations with two potentials [7—9].

The results from the numerical modelling of the dipole magnet are given in Figs.3—6. The central field is 0.75 T. Figure 3 shows the distribution of the main field component B_y along the z axis. The center of the magnet corresponds to the point with coordinates $x = y = z = 0$.

A close agreement between the results obtained by using the two different independent approaches demonstrates the accuracy of the computations.

Figure 4 presents the distribution of the B_y and B_z field components in the plane of $x = 0$ inside the magnet aperture. Figure 5 shows the behaviour of the B_y field component for the plane of $y = 0$. In Fig.6 the distribution of the magnetic field is given for the plane of $x = y$ (the angle in the plane OXY is equal to 45°). The current in one coil and the current density used in the computations were 1.347 MA and 5588.18 A/cm^2, respectively.

Table 2 presents the field integrals of $\int B_y dl$ inside the magnet aperture along the rays from the center of the L3 magnet in the polar coordinate system.

Table 2. Field integrals of the dipole magnet

$\int B_y dl (T \cdot m)$	$\theta = 0°$	$\theta = 2°$	$\theta = 7.5°$	$\theta = 9°$
$\varphi = 0°$	2.79	2.84	3.56	3.71
$\varphi = 45°$	2.79	2.80	2.99	3.02
$\varphi = 90°$	2.79	2.77	2.68	2.74

4. Coil

The main design parameters of the coil are given in Table 1 and the design in Figs. 1, 2, 7. The coil is made of a conductor with an Al matrix of high purity (see Table 3). The double-layer saddle shaped coil has a cylindrical aperture. Windings 1 (Fig.7) are placed inside the support cylinder 8 made of Al sheets and fastened with the help of Al flanges 3. The technique for winding and stacking into the auxiliary support cylinder consists in the

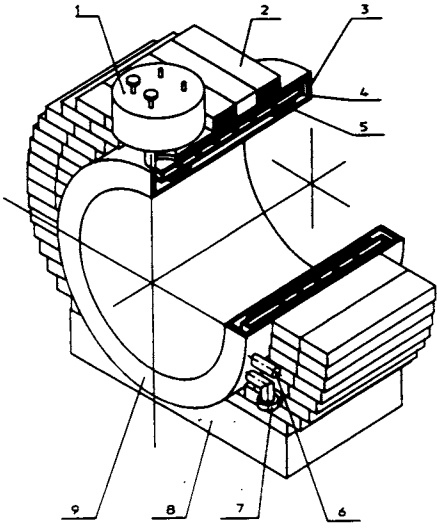

Fig.1. Dipole magnet assembly: 1 — cold box; 2 — iron yoke; 3 — vacuum vessel; 4 — support cylinder; 5 — SC coil; 6 — current leads; 7 — vacuum pumping line; 8 — base; 9 — cryostat

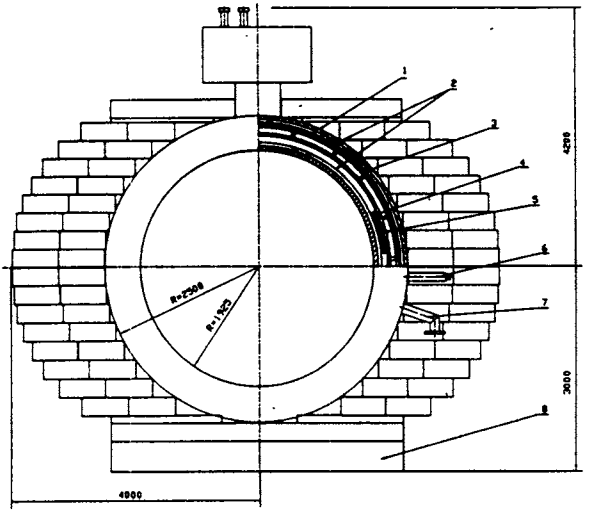

Fig.2. Dipole magnet cross section: 1 — vacuum vessel; 2 — radiation shields; 3 — support cylinder; 4 — helium pipes; 5 — SC coil; 6 — current leads; 7 — vacuum pumping line; 8 — base

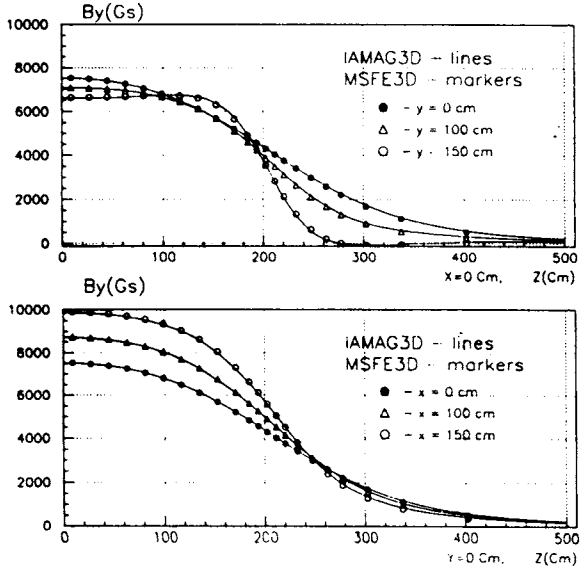

Fig.3. B_y field component computed by means of two codes for the dipole magnet

Fig.4. B_y and B_z field components of the dipole magnet for the plane $x = 0$

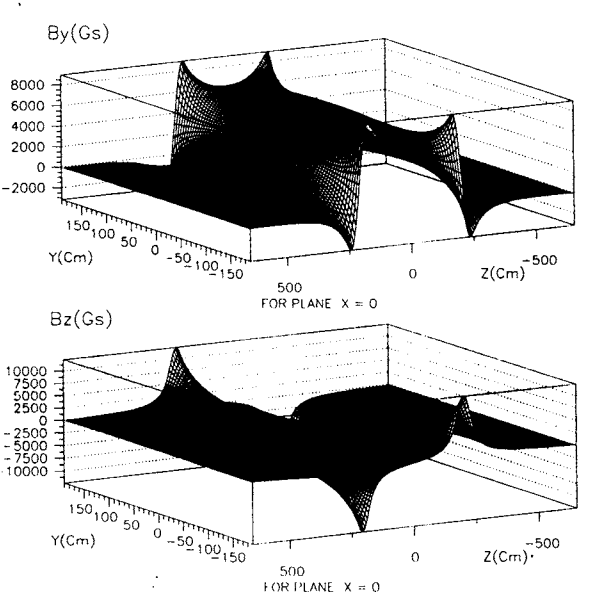

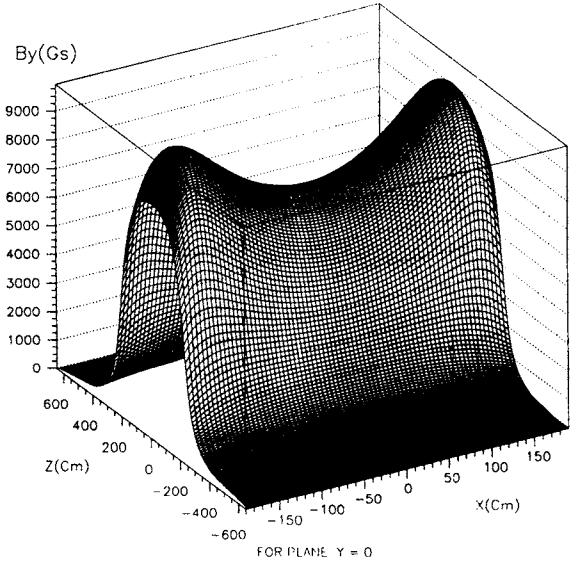

Fig.5. B_y field component of the dipole magnet for the plane $y = 0$

following steps: 1 — the isolation of the conductor by a pre-cured epoxy strip; 2 — winding the conductor on a whirligig machine with a swinging intermediate auxiliary frame; 3 — transferring the winding (1 or 2 layers) inwards the support cylinder and strengthening with screws and flanges; 4 — wrapping up the support cylinder and the winding in thermal insulation and heating up to 120°C. The first extracts the epoxy resin from the preprepared foil and then causes polymerization. Thus, the winding becomes

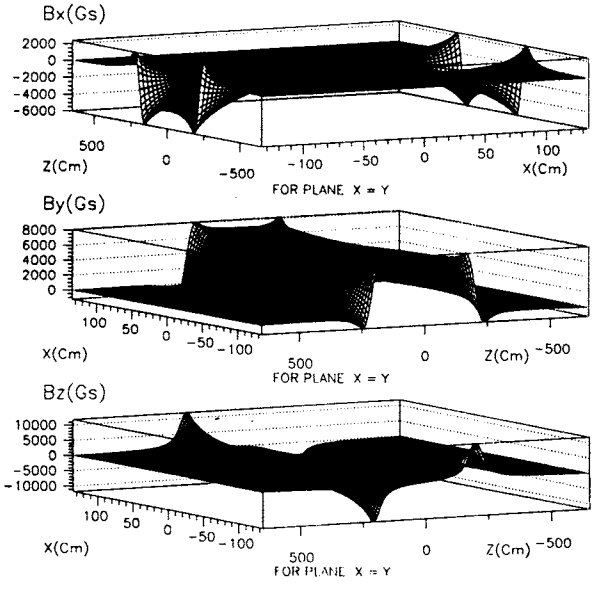

Fig.6. Field components of the dipole magnet for the plane $x = y$ (angle = 45°)

Fig.7. Cross section at the end of the dipole magnet: 1 — SC coil; 2, 7 — LHe cooling pipes; 3 — flange; 4 — inner shell; 5 — superinsulation; 6 — support of the schield; 8 — support cylinder; 9 — outer shell; 10 — chimney; 11 — GHe cooling pipes; 12 — end plate of the vacuum vessel

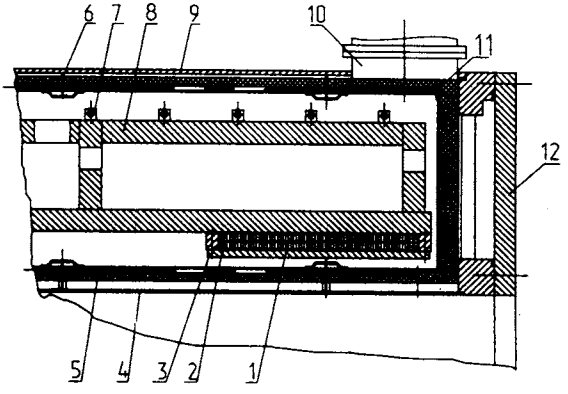

monolithic and is firmly bonded with the support cylinder. The usage of such technology does not require a high accuracy of surface manufacturing for the winding and the support cylinder since a «dry» winding readily takes the form of support cylinder. The support cylinder is suspended on the supports inside the outer shell of the vacuum vessel.

Conductor

The parameters for the conductor and electrical insulation are listed in Table 3. The choice of materials for the conductor, the ratio of nominal and critical currents and the density of current in the conductors is made on the basis of existing world wide experience.

The choice of the current density j both in the coil and in conductor is determined by the stored energy E. We used the following expression to calculate approximately the current density in the conductor [1]:

$$\ln (j) = -0.192 \ln E + 4.652,$$

where E — in MJ, j — in A · mm^{-2}.

Table 3. Conductor parameters

Component	Characteristic	Unit	Value
Strand	Diameter	mm	1.0
	Ratio NbTi/Cu		1/1.38
	J_c in SC at 5 T, 4.5 K	A/mm^2	≥2000
	Filaments diameter	μm	30
	Twist pitch	mm	25
Cable	Number of strands		12
	Overall dimensions	mm^2	5.8 × 1.8
	Twist pitch	mm	50
Aluminium	RRR (B = 0 T)		>1000
matrix	Purity	%	99.995
Conductor	Overall dimensions	mm^2	24 × 3.6
	Operating current in magnet at 3 T, 4.5 K	A	5000
	Critical current at 3 T, 4.5 K	A	≥10000
	Unit length	km	2.5
	Total length	km	10
Insulation	Material	glass fiber epoxy	
	Thickness:		
	interlayer	mm	1.0
	ground	mm	1.0
	on conductor	mm	0.5

In our case, $j = 58\text{A} \cdot \text{mm}^{-2}$ at $E = 27$ MJ in the conductor.

The conductor is a flat superconducting cable inside the high purity Al matrix. The chosen value of the operating current corresponds to a temperature margin of 2.5 K and an enthalpy margin of $\approx 3400\ J/\text{m}^3$.

In case of ramping the magnetic field in the dipole magnet during daily operation in accordance with the LHC beam injection and acceleration, the electrical conductivity of

high purity Al will become lower. It is a known effect that the specific electrical resistance of pure aluminium at a cryogenic temperature is strongly dependent on the values of relative deformations and the number of cycles, respectively [12]. So, these deformations should be kept low (<<0,1%). It will require appropriate changes in the design of the coil.

Support Cylinder

The support cylinder (see Figs.2 and 7) is made of two coaxial cylinders and ribs, connected between themselves by an argone-arc welding procedure. It is made of an aluminium alloy with the following features:

$$\sigma_B = 537 \text{ MPa}, \sigma_{0.2} = 215 \text{ MPa at } 20 \text{ K } [10].$$

The winding located in the aperture of the cylinder is attached by bolts with the help of flanges (see Fig.7). According to the calculated results obtained with the SUPERFISH 2D-code, the electromagnetic forces acting on the cylinder from the winding are basically in the horizontal plane and equal to $F_e = 1.46 \cdot 10^5$ kgs/m. The radial thicknesses of the support cylinder, the inner and outer shells were estimated on the basis of allowable values for the relative deformation $\varepsilon = 0.1\%$ and $\sigma = 80$ MPa.

The achievement of the value of $\varepsilon << 0.1\%$ would be very desirable provided the magnet is switched on and off a few times a day. If it is typical for the operation of the magnet, then the proper solution would be to introduce thermally isolated supports between the basis cylinder and the outer shell of the vacuum vessel. Thus electromagnetic forces will be kept on the iron yoke.

5. Cryostat

The cryostat consists of a vacuum vessel, radiation shields with multilayer thermal insulation and tubes for liquid and gaseous helium (see Figs.1, 2 and 7 and Table 1). The cold box containing liquid helium is attached to the cryostat.

The vacuum vessel has a cylindrical shape with two detachable end plates (see Fig.7). It is made of stainless steel. The cold mass is estimated to be 25 t. The vacuum vessel should withstand the weight above and uncompensated forces between the coil and the iron yoke, and between the L3 magnet and the dipole magnet.

The location of supports (1 and 2), holding support cylinder (4) with windings inside vacuum vessel (3), is shown in Fig.8. The desing of the axial support is seen in Fig.9. These supports maintain a constant position for the axis of the support cylinder during cooling. The thermal isolation part of the supports consists of a fiberglass tude, a thermal intercept connected to the radiation shield, and a carbon fiber tube (see Fig.9). The heads of the supports are attached to the vacuum vessel and the support cylinder via hinges.

Fig.8. Dipole magnet cryostat cross section: 1 — radial supports (12 at each end); 2 — axial supports (6 at one end); 3 — vacuum vessel; 4 — coils with a support cylinder; 5 — radiation shields

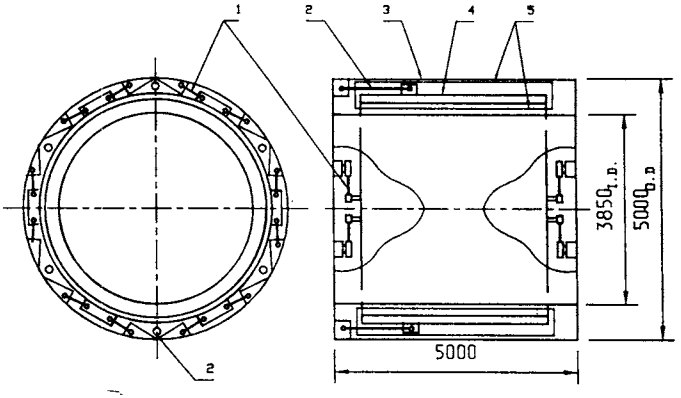

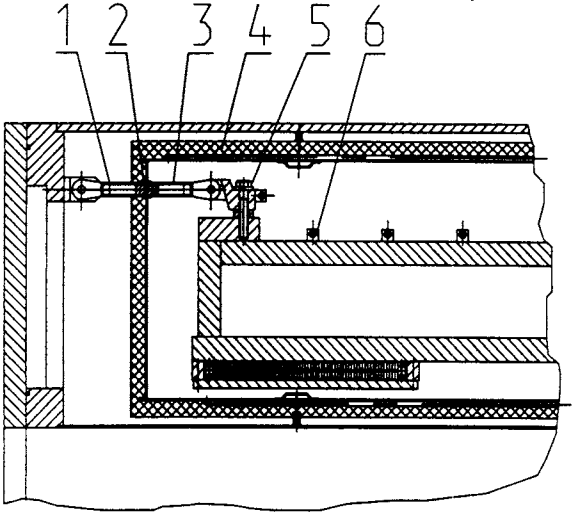

Fig.9. Section view of support: 1 — G10; 2 — 80 K intercept; 3 — GRP carbon fiber tube; 4 — 80 K shield + MLI; 5 — stell washers; 6 — LHe pipe

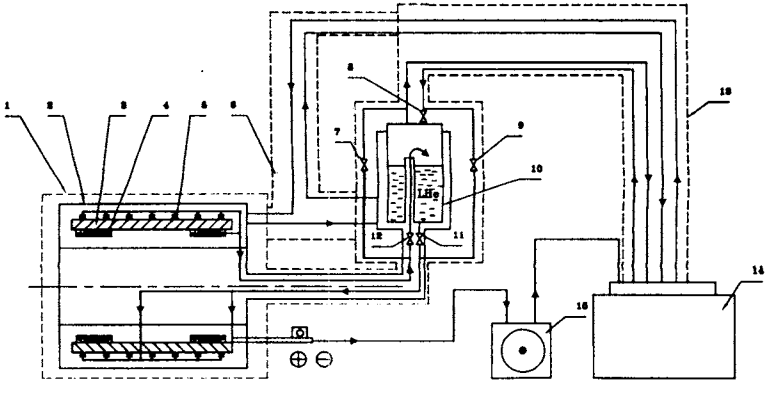

Fig.10. Schematic diagram of the helium flow: 1 — vacuum walls; 2 — radiation shields; 3 — support cylinder; 4 — SC coil and LHe pipes; 5 — LHe pipes; 6 — GHe cooling pipes; 7—9, 11, 12 — valves; 10 — cold box; 13 — He transfer line; 14 — He refrigerator; 15 — He compressor

The radiation shields made of 5 mm thick sheets of aluminium alloy are attached to the walls of the vacuum vessel (see Fig.7). Liquid helium at 50 K flows through the tubes welded to these sheets. The joints of the radiation shields are allowed to have some thermal deformations. To reduce an influence of eddy currents arising from changes of the magnetic field, the shields are divided into parts fastened to each other with electrical-insulation plates.

The multilayer thermal insulation consists of double layers of SNT-10 synthetic paper 10 thick and AD-1 aluminium foil 10 μm thick. There are 20 double layers of such insulation around the surface of the support cylinder (outside and inside), and 80 double layers are connected to thermal screens. The thermal conducting aluminium tape of Scotch 3M-425 is also considered for use [13].

6. Refrigeration System

Vacuum System

The vacuum volume of the cryostat is of the order of 40 m^3. Due to a large amount of superinsulation layers used for the radiation shields, the pumping of the volume requires a series of pumps to reach the needed vacuum.

The initial vacuum pumping from $P = 1$ bar to $P = 50$ mbar is reached by a mechanical pump. Then, booster vacuum pumps will pump a volume to 10^{-1} mbar. At the final stage, a diffusion pump is switched on, and a necessary vacuum of about $10^{-6} - 10^{-7}$ mbar is reached.

Cryogenics

A block-diagram of the refrigeration system is shown in Fig.10.

The winding is indirectly cooled using the thermosyphon circulation of a two-phase helium flow through the cooling tubes. Safe cool-down to 4.5 K with a temperature gradient of 40 K across the winding can be done for 120—140 hours with a helium mass flow of 20 g/s using the latent heat of helium vaporization and the enthalpy of helium gas.

The full cryogenic system requires a helium flow of 3 g/s during steady-state operation at 4.5 K, assuming heat leaks into the winding and the chimney and cooling two current leads with a liquid helium consumption of 0.5 g/s. A helium flow of 2 g/s with a temperature of 40 K from the helium refrigerator is required for a 80 K thermal shield (the use of the cryogenic scheme with cryocoolers [14] could be considered later).

An additional helium flow of ~5 g/s is required during magnet current ramping. After magnet quench with an energy removal of 50% the recovery procedure requires about 12 hours, and in the worst case, if all the energy is discharged in the magnet, this procedure requires about 20 hours to cool down the winding from 85 K. Some additional heat leaks

(about ~20%) into the liquid helium are possible from: a helium transfer line, valves and other equipment.

7. Power Supply and Quench Protection

The power supply, developed at CERN (Geneva), consists of two modules of 24 KW with a maximum voltage of 8 V at 6 kA connected in parallel.

The electrical circuit consists of two series-connected double-layer coils, helium vapour cooled current leads, a power supply, and two current switches.

The fast system, used to detect the resistive state in the winding, can be ensured by a bridge scheme detection.

At the evacuation of energy from the magnet, these coils are connected to a dump resistor. In the case of fast evacuation, the initial voltage on the dump resistor will be about 500 V, and in the case of slow evacuation it will be about 40—50 V. Thyristor and mechanical switches will be used.

Two independent detectors of occurrence of normal zones will be used for reliability. In the case of failure of the quench protection device and discharging the full energy E over the cold mass, the final temperature from heating the coil with mass M_{coil} and cold mass M will be between two extreme values:

1) $E/M \cong H(T_{max})$, where H is the enthalpy of aluminium.

$$E/M = 27 \cdot 10^3 \text{ kJ}/25 \cdot 10^3 \text{ kg} = 1.08 \text{ kJ/kg},$$

which corresponds to $T_{max} = 43$ K.

2) $E/M_{coil} = 27 \cdot 10^3/2.5 \cdot 10^3 = 10.8$ kJ/kg,

and $T_{max} = 85$ K.

In both cases, there will be no essential deformations of the coil.

A pair of 5-kA current leads will be used in the dipole magnet. The specific heat influx to the helium at the nominal current is 1 W/kA; the hydraulic resistance, 10 kPa; and the electrical insulation strength, 10 kV. The current-carrying element (heat exchanger part) consists of flattened copper shields installed between two copper strips. The stack is butt-welded along its entire length. This type of current-carrying element has been used for the force-cooled current leads in the superconducting magnets at the Laboratory of High Energies, JINR (Dubna) over a long period of time [15].

These current leads have a high reliability, compactness, a low heat influx, and a low hydraulic resistance. For example, the cross section of the current-carrying element

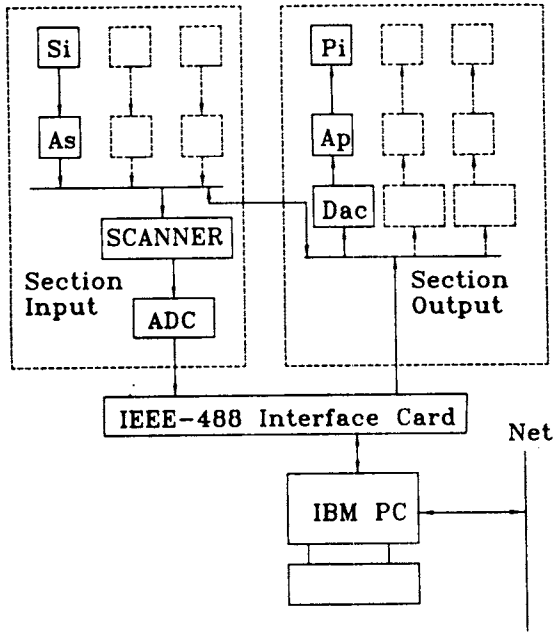

Fig.11. Control and monitoring system of the superconducting dipole magnet

of a 6 kA current lead is 28 · 15 mm^2; the effective length, 600 mm; and the He specific cooling surface, 55 $cm^2 \cdot cm^{-3}$.

8. Control Instrumentation

A function diagram of the control and monitoring system of the magnet is shown in Fig.11. The system controls all the parameters relevant to the operation of the magnet including: temperatures, pressures, He flow rates, vacuum, voltages, etc.

The circuit includes a front-end section with sensors (Si) and transducers (As) and an output section with transducers (Ap) and executive devices (Pi). Both sections are connected through an IEEE-488 Interface card to a computer. The computer is connected to a general ALICE control system. The unique feature of the system is the fact that a signal from any gauge is at once scaled to a single range of values, and as a current signal, it is transferred through an ADC scanner to the computer. Similarly, all executive devices operate through the transducers with input signals over a range of 10 to 100 mA. This approach not only simplifies the system and increases its reliability, but also allows the transfer of signals at a hardware level at a maximum speed from the gauges to the executive devices.

The system contains about 70 gauges of 10 different types and 5 managing executive devices. As a basis of the electronic system, the GPIB standard was chosen on the IBM-PC computer platform and the LabView software.

The system is capable of performing the following functions:

1. testing individual subsystems during the magnet construction,
2. testing the magnet before comissioning,
3. control and monitoring during the comissioning,
4. control and monitoring the parameters of the magnet during the operation,
5. ensurance of the protection functions in the case of failures.

9. Conclusion

The authors would like to express their gratitude to Prof. A.M.Baldin, Drs. A.D.Kovalenko and Yu.K.Pilipenko from JINR for their support of this work, to Drs. J.Schukraft, W.Klempt, L.Leistam and D.Swoboda from the ALICE Collaboration and Drs. J.Schmid, G.Passardi, N.Delruelle and F.Haug from the CERN cryogenics group for fluitful discussions. The authors would like to thank Dr. J.Demko for his help in this work.

References

1. Ahmad N. et al. — ALICE, Technical Proposal for a Large Ion Collider Experiment at the CERN LHC. CERN/LHCC 95-71, Geneva, 1995.
2. Borisovskaya Z.V., Datskov V.I., Eggert K. et al. — Magnet System of ALICE Forward Muon and *pp* Spectrometer. Internal Note ALICE/95-08, 1995.
3. Dudragne A., Fabian C.W., Flegel W. et al. — A Shaped Solenoid for Muon Spectroscopy at High Energy Hadron Colliders. CERN-PPE/92-101, 17 June 1992.
   Borisovskaya Z.V., Shelaev I.A., Shishov Y.A. et al. — The Large ALICE Magnet System. Internal Note ALICE/93-23, 1993.
   Borisovskaya Z.V., Flegel W., Mironov S.V. et al. — NIM, 1995, vol.A365, p.329-336.
4. Akishin P.G. — JINR, P11-86-522, Dubna, 1986 (in Russian).
5. Akishin P.G. — Journal of Computational Mathematics and Mathematical Physics, 1989, vol.29, No.8 (in Russian).
6. Akishin P.G., Zhidkov E.P., Kravtsov V.D. — Mathematical Modeling, 1989, vol.1, No.7, pp.100—107 (in Russian).
7. Yuldasheva M.B., Yuldashev O.I. — JINR, P11-94-202, Dubna, 1994 (in Russian).

8. Zhidkov E.P., Yuldasheva M.B., Yuldashev O.I. — Mathematical Modelling, 1994, vol.6, No.9, pp.99—116 (in Russian).
9. Zhidkov E.P., Yuldasheva M.B., Yudin I.P., Yuldashev O.I. — NIM, 1995, vol.A365, pp.308—316.
10. Gudkov S.I. — The Mechanical Properties of Industrial Coloured Metals at Low Temperatures. «Metallurgy», M., 1971, p.63 (in Russian).
11. Wittgenstein F. — IEEE Transactions on Magnetics, 1992, vol.28, No.1, pp.104—112.
12. Hartwig K.T., Yuan G.S., Lehmann P. — IEEE Trans. on Magnets, 1985, vol. Mag-21, No.2, pp.161—164.
13. Zeller A.F., Kamp J.C. — Long Term Results from the Elimination of MLI between 4 and 77 K. Advances in Cryogenic Engineering, vol.39. Plenum Press. New York, 1994, pp.1691—1697.
14. Kuriyama T. et al. — Abstract Booklet ICEC 15, 1994, p.305.
15. Bartenev V.D., Shishov Yu.A. — Cryogenics, 1991, vol.31, November, pp.985—987.

Received on November 14, 1996.